First-principles study of atomic ordering in fcc Ni-Cr alloys

Moshiour Rahaman,[1] B. Johansson,[2] and A. V. Ruban[1]

[1]*Multiscale Materials Modeling, Department of Materials Science and Engineering, Royal Institute of Technology, SE-100 44 Stockholm, Sweden*

[2]*Applied Material Physics, Department of Materials Science and Engineering, Royal Institute of Technology, SE-100 44 Stockholm, Sweden*

(Received 13 September 2013; revised manuscript received 13 December 2013; published 7 February 2014)

We investigate atomic ordering in fcc Ni-rich Ni-Cr alloys using first-principles techniques and statistical mechanics simulations based on the Ising Hamiltonian with effective cluster interactions computed by the screened generalized perturbation method (SGPM) and projector augmented wave (PAW) method. We demonstrate that effective chemical interactions in this system are quite sensitive to alloy composition and in fact to the specific configurational state. The chemical interactions for the high-temperature random state produce the atomic short-range order (SRO) with intensity maximum close to the $(\frac{2}{3}\frac{2}{3}0)$ point of the reciprocal space in agreement with the previous first-principles investigation. A consistent with diffuse neutron scattering data maximum at the $(1\frac{1}{2}0)$ position is obtained only when we take into consideration relatively small strain-induced interactions, which solves a long-standing inconsistency between theory and experiment in this system. The calculated transition temperature of order-disorder transition of Ni_2Cr alloy, 880 K, is in good agreement with the experimental value of 863 K.

DOI: 10.1103/PhysRevB.89.064103 PACS number(s): 75.50.Bb, 64.90.+b, 71.20.Be, 71.55.Ak

I. INTRODUCTION

Ni-Cr alloys form solid solutions over a wide range of composition and temperature on the fcc lattice [1]. They have an excellent combination of mechanical strength and high-corrosion resistance at elevated temperature, which makes them attractive in a variety of applications such as aircraft gas turbines, steam turbine power plants, chemical and petrochemical industries [2]. At the same time, it is established that some properties, for instance, electrical resistivity and ductility are connected to atomic ordering in this system [3–6], which exhibits quite unusual behavior.

At low temperatures, fcc Ni-rich random alloys become unstable and a first-order phase transition occurs to the Pt_2Mo-type ordered structure [7–11] with the highest transition temperature of 863 K at the stoichiometric alloy composition, Ni_2Cr. It is characterized by superstructure vector $(\frac{2}{3}\frac{2}{3}0)$ [or $\frac{4}{3}(1\frac{1}{2}0)$] in the reciprocal space. The fact that the latter is shifted from the fcc $(1\frac{1}{2}0)$ special point where the diffuse scattering SRO maxima of random Ni-Cr alloys is observed, has attracted much attention to the mechanism of the phase transformation in Ni-Cr and other similar systems [12–15].

The atomic SRO in fcc Ni-Cr random alloys has been extensively studied experimentally. Diffuse neutron scattering technique was used by Vintaykin *et al.* [16,17] for $Ni_{0.67}Cr_{0.33}$ alloys and by Caudron *et al.* [18,19] for $Ni_{0.67}Cr_{0.33}$ and $Ni_{0.75}Cr_{0.25}$. Schönfeld *et al.* [20,21] and Schweika and Haubold [22] studied the atomic SRO and static atomic displacements in $Ni_{0.8}Cr_{0.2}$ and $Ni_{0.89}Cr_{0.11}$ using the diffuse neutron scattering and synchrotron radiation. They also evaluated effective pair interactions in this system using both the Krivoglaz-Clapp-Moss equations and the inverse Monte Carlo method.

As for theoretical investigations, there exist two *ab initio* studies of the SRO in Ni-Cr alloys [23,24]. However, their results are quite controversial. Turchi *et al.* [23] calculated effective cluster interactions (ECI) by the generalized perturbation method (GPM) implemented in the first-principles framework of the Korringa-Kohn-Rostocker (KKR) method and the coherent potential approximation (CPA). They got negative nearest-neighbor effective pair interaction, which lead to a phase separation instead of ordering.

Staunton *et al.* [24] using the $S^{(2)}$ formalism within the same KKR-CPA method for the effective interactions and a mean-filed method within an Onsager cavity-field approach, demonstrated that the problem with interactions in the calculations by Turchi *et al.* [23] was related to the neglect of charge transfer in the GPM calculations. At the same time, although the problem with a phase separation trend was solved in Ref. [24], the resulting theoretical diffuse intensity map in the reciprocal space had additional maxima at $(\frac{2}{3}\frac{2}{3}0)$ at variance with the existing experimental data.

In this work, we study atomic ordering in Ni-rich Ni-Cr alloys using several different *ab initio* techniques. In particular, we use the SGPM [25,26], which is a GPM method adopted to the density functional theory (DFT) first-principles calculations by including a contribution from the screened Coulomb interactions [25,27] and the full-potential PAW method [28] for calculating strain-induced interactions. The statistical modeling is done by the Monte Carlo (MC) method.

II. METHODOLOGY

A. Configurational Hamiltonian

We use an Ising Hamiltonian for a statistical thermodynamic description of alloy energetics on a lattice, which presents the configurational energy of an alloy in terms effective cluster interactions:

$$E_{\rm conf} = \frac{1}{2}\sum_p V_p^{(2)} \sum_{i,j\in p} \delta c_i \delta c_j + \frac{1}{3}\sum_t V_t^{(3)} \sum_{i,j,k\in t} \delta c_i \delta c_j \delta c_k + \frac{1}{4}\sum_q V_q^{(4)} \sum_{ijk\ell\in q} \delta c_i \delta c_j \delta c_k \delta c_\ell. \quad (1)$$

Here, $V_s^{(n)}$ are the n-site ECI for the cluster of an s type, δc_i are the concentration fluctuations at sites i: $\delta c_i = c_i - c$, where c_i is the occupation number at site i, taking on values 1 or 0 if the site i is occupied by Ni or Cr atom, respectively, and c is the concentration of Ni. The summation in (1) is carried out over all sites.

The ordering energy, i.e., the difference of the energies of the ordered and random alloys for a fixed lattice constant in terms of the ECI is expressed as

$$\Delta E_{\text{ord}} = \frac{1}{2} c(1-c) \sum_p z_p V_p^{(2)} \alpha_p + \text{h.o.t.} \tag{2}$$

Here, the first term is the contribution from effective pair interactions (EPI) expressed using the Warren-Cowley SRO parameters: $\alpha_p = (\langle c_i c_j \rangle - c^2)[c(1-c)]^{-1}$; for the pth coordination shell, z_p is the coordination number for the pth coordination shell and h.o.t. stands for the contribution from the higher-order or multisite interactions.

B. Static concentration wave method

In the static concentration wave method [29], the contribution from the EPI to the ordering energy is determined as

$$\begin{aligned} \Delta E_{\text{ord}} &= \frac{1}{2} c(1-c) \frac{\Omega_0}{(2\pi)^3} \int_{BZ} d\mathbf{q} V_{\mathbf{q}} \alpha_{\mathbf{q}} \\ &= \frac{1}{2} \frac{\Omega_0}{(2\pi)^3} \int_{BZ} d\mathbf{q} V_{\mathbf{q}} |c_{\mathbf{q}}|^2, \end{aligned} \tag{3}$$

where Ω_0 is the volume of primitive unit cell, $V_{\mathbf{q}}$, $\alpha_{\mathbf{q}}$, and $c_{\mathbf{q}}$ are the Fourier transforms of the EPI, short-range order parameter, and concentration fluctuations, respectively:

$$\begin{aligned} V_{\mathbf{q}} &= \sum_p \sum_{i \in p} V_p^{(2)} e^{-i\mathbf{q}R_i}, \\ \alpha_{\mathbf{q}} &= \sum_p \sum_{i \in p} \alpha_p e^{-i\mathbf{q}R_i}, \\ c_{\mathbf{q}} &= \sum_i \delta c_i e^{-i\mathbf{q}R_i}. \end{aligned} \tag{4}$$

It is clear from (4) that $\alpha_{\mathbf{q}} = |c_{\mathbf{q}}|^2$. Both of them satisfy the sum rule:

$$\frac{\Omega_0}{(2\pi)^3} \int_{\mathbf{BZ}} d\mathbf{q} \alpha_{\mathbf{q}} = \frac{1}{c(1-c)} \frac{\Omega_0}{(2\pi)^3} \int_{\mathbf{BZ}} d\mathbf{q} |c_{\mathbf{q}}|^2 = 1, \tag{5}$$

which plays an important role in the statistical theory of ordering.

The alloy configuration in this formalism is given by a superposition of the static concentration waves with amplitudes, $c_{\mathbf{q}}$, or Fourier transforms of the SRO parameters, $\alpha_{\mathbf{q}}$. At finite temperature, the latter can be found from a minimization of the corresponding free energy functional, which leads to the Krivoglaz-Clapp-Moss type equation [30–32] connecting the Fourier transforms of the EPIs, $V_{\mathbf{q}}$ and SRO parameters $\alpha_{\mathbf{q}}$, which, for instance, in the ring mean-field approximation of the thermodynamic fluctuation method is [33]

$$\alpha_{\mathbf{q}} = \left[1 + \frac{c(1-c)}{k_B T} (\mu + V_{\mathbf{q}}) \right]^{-1}, \tag{6}$$

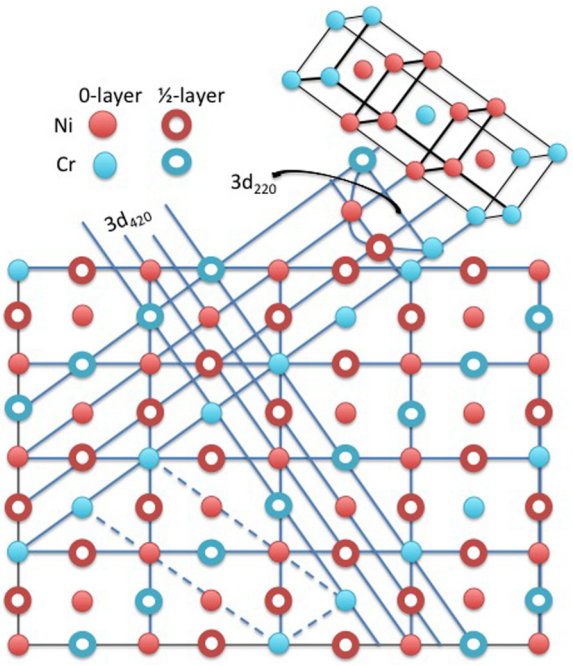

FIG. 1. (Color online) The ordered structure of Ni_2Cr with projection of atoms on the (001) plane.

where, μ is the chemical potential is determined from the sum rule (5).

It follows from Eq. (6) that the positions of the maximum of the Fourier transform of the SRO parameters and the minimum of $V_{\mathbf{q}}$ should coincide. Therefore, just knowing $V_{\mathbf{q}}$, one can predict the type of the atomic SRO in the random state. As has been already mentioned, the maximum of $\alpha_{\mathbf{q}}$ in the Ni-rich Ni-Cr alloys is observed at the fcc special $(1\frac{1}{2}0)$ point, so this should be also the position of the minimum of the Fourier transform of the EPI.

The formation of the long-range ordered structure happens in a somewhat different way. In this case, the alloy composition and crystal structure impose additional boundary conditions and therefore the ground state structure can be presented by the concentration wave(s) with wave vectors $\mathbf{q}$ different from the position of the minimum of $V_{\mathbf{q}}$. This is the case of the Ni_2Cr phase where the static concentration wave is formed by superstructure vector $(\frac{2}{3}\frac{2}{3}0)$ [or equivalently $\frac{4}{3}(1\frac{1}{2}0)$], which is different from $(1\frac{1}{2}0)$.

In Fig. 1, we show the Ni_2Cr ordered structure as the "Cr-Ni-Ni-Cr" stacking sequence of either the (420) or (220) planes with every third plane containing only Cr and two others only Ni atoms. In the completely ordered state, the site occupation in the Ni_2Cr structure is determined by the following concentration wave [29]:

$$\begin{aligned} c(\mathbf{R}) &= \frac{1}{3} + \frac{2}{3} \cos\left[\frac{4\pi}{3} (2x + y) \right] \\ &= \frac{1}{3} + \frac{2}{3} \cos\left[\frac{4\pi}{3} (x + y) \right], \end{aligned} \tag{7}$$

where $\mathbf{R}$ is the fcc lattice vector, and x and y are $x-$ and $y-$components of $\mathbf{R}$ in units of the lattice constant.

C. First-principles calculations

Ab initio calculations have been done by the exact muffin-tin orbitals (EMTO) [34–36] and PAW [28,37] methods using DFT [38]. The PAW method [28] has been used as is implemented in the Vienna *ab initio* simulation package (VASP) [37], in the calculations of the enthalpies of formation of ordered alloys, relaxation energies, forces and local lattice displacements using the generalized gradient approximation (GGA) [39]. The energy cutoff was 300 eV.

In all the calculations presented here, we have neglected the spin-polarization, since the main focus is on the description of the alloy configuration at temperatures above 800 K, although magnetic phase transition in Ni is at about 660 K and it disappears together with low-temperature local magnetic moment already when concentration of Cr is about 11 at.% [40]. The local magnetic moment on Ni and Cr atoms can exist at high temperatures due to longitudinal spin fluctuations, however, its effect upon the chemical bonding related to ordering is supposed to be small and will be neglected here.

The local density approximation (LDA) [41] has been used for the exchange-correlation potential in the EMTO DFT self-consistent calculations, while the total energy has been obtained in the GGA [39]. All the EMTO calculations were performed using an orbital momentum cutoff of $l_{\max} = 3$ for partial waves. The ECI has been calculated at the corresponding experimental lattice parameters [1,11,42–44].

The electronic structure of random alloys has been calculated within the CPA [45,46]. In the CPA-DFT calculations, the contribution of the screened Coulomb interactions to the one-electron potential of alloy components, $V^i_{\rm scr}$, and to the total energy, $E_{\rm scr}$, has been taken into consideration [25]:

$$V^i_{\rm scr} = -e^2\alpha_{\rm scr}\frac{q_i}{S}, \qquad E^i_{\rm scr} = -e^2\frac{1}{2}\alpha_{\rm scr}\beta_{\rm scr}\frac{q_i^2}{S}. \tag{8}$$

Here, q_i is the net charge of the atomic sphere of the ith alloy component, S is the Wigner-Seitz radius, $\alpha_{\rm scr}$ and $\beta_{\rm scr}$ are the on-site screening constants.

The screening parameters, α and β, were evaluated from 864-atom supercell calculations of random Ni_xCr_{1-x} alloys using the locally self-consistent Green's function (LSGF) method [47], which has also been used to study local environment effects in the electronic structure and effective interactions in Ni-Cr alloys. Their values are $\alpha_{\rm scr} = 0.794, 0.785, 0.773$ and $\beta_{\rm scr} = 1.15, 1.147, 1.144$, for random $Ni_{0.67}Cr_{0.33}$, $Ni_{0.75}Cr_{0.25}$, and $Ni_{0.8}Cr_{0.2}$ alloys, respectively.

The integration over the Brillouin zone for Ni_xCr_{1-x} random alloys has been performed using a $31 \times 31 \times 31$ grid of special $\mathbf{k}$ points determined according to the Monkhorst-Pack scheme [48]. In the case of ordered alloys, an equivalent grid of $\mathbf{k}$ points has been used in the corresponding integration over the Brillouin zone.

D. Effective cluster interactions: chemical contribution

The ECI of the Ising Hamiltonian have been calculated by the SGPM [25–27]. The SGPM yields only the "chemical" part of the effective interactions, i.e., the ECI on the fixed (unrelaxed) underlying crystal lattice. The contribution from the strain-induced interactions due to local lattice relaxations has been considered separately within the framework of the microscopic elastic theory as is described below.

The SGPM EPI for the pth coordination shell is defined as [25,26]

$$V_p^{(2)-\rm ch} = V_p^{\rm one\text{-}el} + V_p^{\rm scr}, \tag{9}$$

where $V_p^{(2)-\rm ch}$ is the total effective interaction, $V_p^{\rm one\text{-}el}$ the one electron contribution, or GPM interaction, and $V_p^{\rm scr}$ the contribution from the screened Coulomb interaction, which can be determined as

$$V_p^{\rm scr} = e^2\alpha_p^{\rm scr}\frac{q_{\rm eff}^2}{S}, \tag{10}$$

where $q_{\rm eff} = q_A - q_B$ is the effective charge transfer. The intersite screening constants $\alpha_p^{\rm scr}$ have been determined in the supercell calculations by the LSGF method as described in Ref. [25]. There is no electrostatic contribution in the case of multisite ECI.

E. Strain-induced interactions

To obtain an additional contribution to the ECI due to local lattice relaxations, we have used a microscopic elastic theory formalism for the strain-induced interactions [49–51]. Within this method it is assumed that elastic and vibrational properties of an alloy can be described by the homogeneous single-site effective medium, so the interactions of alloy components are considered as its perturbation. It is also assumed that atomic lattice displacements are relatively small so that the harmonic approximation is valid.

Then, the minimization of the elastic energy with respect to the local lattice displacements leads to the following expression for the Fourier transform of the pair stain-induced interactions [49,50]:

$$V^{\rm si}(\mathbf{q}) = u(\mathbf{q})F^*(\mathbf{q}), \tag{11}$$

where $u(\mathbf{q})$ and $F(\mathbf{q})$ are the Fourier transforms of local lattice displacements $\mathbf{u}_i$ and Kanzaki forces $\mathbf{F}_i$ at site i, respectively. Then the pair strain-induced interactions in the real space are

$$V^{\rm si}(\mathbf{R}_p) = \frac{1}{N_q}\sum_{\mathbf{q}} V^{\rm si}(\mathbf{q})\exp(i\mathbf{q}\mathbf{R}_p), \tag{12}$$

where N_q is the number of $\mathbf{q}$ points in the summation. Alternatively, but equivalently, the strain-induced interactions can be directly calculated in the real space from the displacements and Kanzaki forces as described in Ref. [52]. So, in the end, the total EPI at the pth coordination shell, $V_p^{(2)}$, is

$$V_p^{(2)} = V_p^{(2)-\rm ch} + V^{\rm si}(\mathbf{R}_p). \tag{13}$$

Since it is a highly nontrivial task to use this formalism within first-principles calculations for concentrated alloys, we have determined the strain-induced interactions in the dilute limit of Cr in Ni. In this case, a single-impurity calculation allows one to determine the Kanzaki (or Hellmann-Feynman in this particular case) forces $\mathbf{F}_i$ (before relaxation) and local displacements $\mathbf{u}_i$ (after relaxation) of the host atoms.

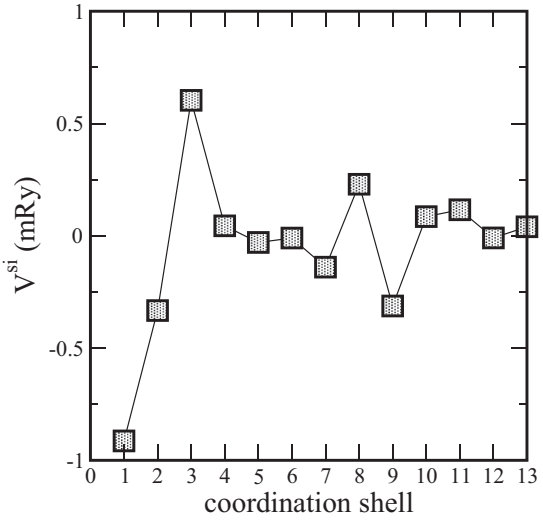

FIG. 2. Strain-induced interactions obtained in the dilute limit of Cr in Ni using Eq. (12).

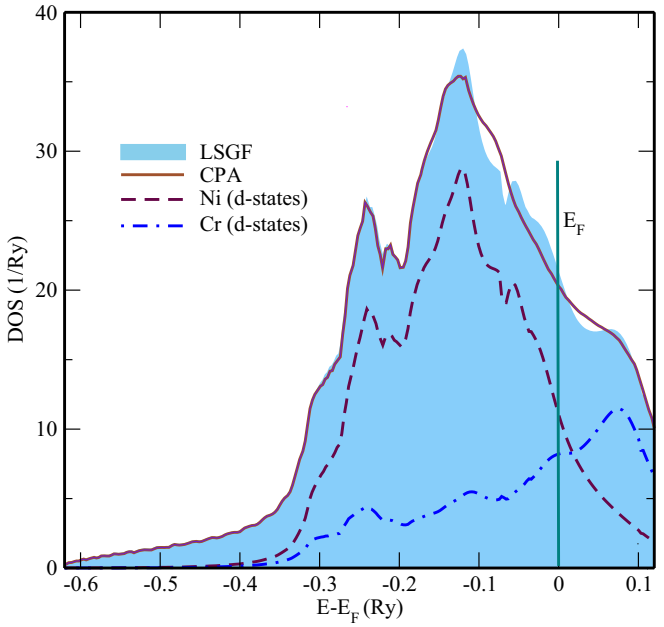

FIG. 3. (Color online) Density of states in the $Ni_{0.67}Cr_{0.33}$ random alloy obtained using the CPA and in the 864-atom supercell LSGF calculations. Ni and Cr partial density of states are shown by dashed and dashed-dotted lines, respectively.

The PAW method [28,37] was employed to obtain the forces and local atomic displacements around Cr impurity in a 256-atom fcc supercell built upon four-atom fcc cubic unit cell $[4 \times 4 \times 4(\times 4)]$ of Ni. The integration over the Brillouin zone has been done using the $4 \times 4 \times 4$ Monkhorst-Pack grid [48]. In Fig. 2, we show the calculated strain-induced interactions.

Let us note that although it is less accurate method compared to their direct calculations, as has been done, for instance, in Ref. [53], it allows to get a long-range tail of the strain-induced interactions, which is important in this case. In fact, due to a small size mismatch of Ni and Cr atoms, the strain-induced interactions are relatively weak compared with the chemical ones. However, their contribution is very important for a correct description of ordering in NiCr.

III. RESULTS AND DISCUSSION

A. Electronic structure of random NiCr alloys

Being based on the single-site approximation, the CPA suffers from various limitations, such as its inability to account for the effects of SRO and the effect of many-site statistical fluctuations. The latter are usually important in systems where partial bands of alloy components have a restricted overlapping, which is just the case of Ni and Cr d-bands in NiCr alloys. Therefore, in order to test the accuracy of the CPA for Ni-Cr alloys, we have calculated the density of states (DOS) of a random $Ni_{0.67}Cr_{0.33}$ alloy using the CPA and the LSGF method.

The LSGF method is an accurate first-principles tool for the total energy and electronic structure calculations of random alloys. Using a big enough supercell, one can take care of the most important atomic distribution correlation functions within the needed range and then calculate its electronic structure. The local interaction zone (LIZ) in the LSGF method allows one effectively to cut the long-range (infinite in fact) interactions thereby retaining the correct properties of electronic spectrum of random alloys. On the other hand, all the local environment effects are taken into consideration within the LIZ, which also allows one to consider systems with atomic SRO.

In Fig. 3, we compare the DOS of the $Ni_{0.67}Cr_{0.33}$ random alloy obtained in the CPA and 864-atom LSGF calculations with LIZ = 3, which means that the electronic correlations within the first two coordination shells are taken into account. The experimental lattice parameter, 3.566 Å [1,42], was used for the calculation of the DOS. As can be seen in Fig. 3, the local environment effects are indeed quit important in Ni-Cr alloys: the DOS obtained within the CPA and using the LSGF differ in the energy range close to the Fermi energy.

The origin of the local environment effects, as has been mentioned above, is a quite distant position of the Ni and Cr d-states, as one can see in Fig. 3. Local fluctuations of composition in such a case lead to the appearance of new features in the DOS, which are not properly presented in the single-site approximation, where the local environment is fixed to the average one. Nevertheless, we proceed with calculations of the effective interactions within the CPA, since the CPA DOS deviates insignificantly from the accurate one, and besides, although the local environment effect can be important for interactions as we will be shown below, the effective interactions are quite accurate on average.

Finally, we would like to demonstrate the effect of the atomic SRO on the DOS. For that purpose we calculate the DOS of the $Ni_{0.67}Cr_{0.33}$ random alloy with nonzero Warren-Cowley SRO parameters at the first two coordination shells, which are approximately equal to -0.1 and 0.1 using the LSGF method with LIZ = 3. The latter corresponds to the atomic SRO in this alloy at about 1000 K [18]. As one can see in Fig. 4, such an atomic SRO leads to a more pronounced peak close to the Fermi level, however, the effect of the SRO on the DOS is relatively small.

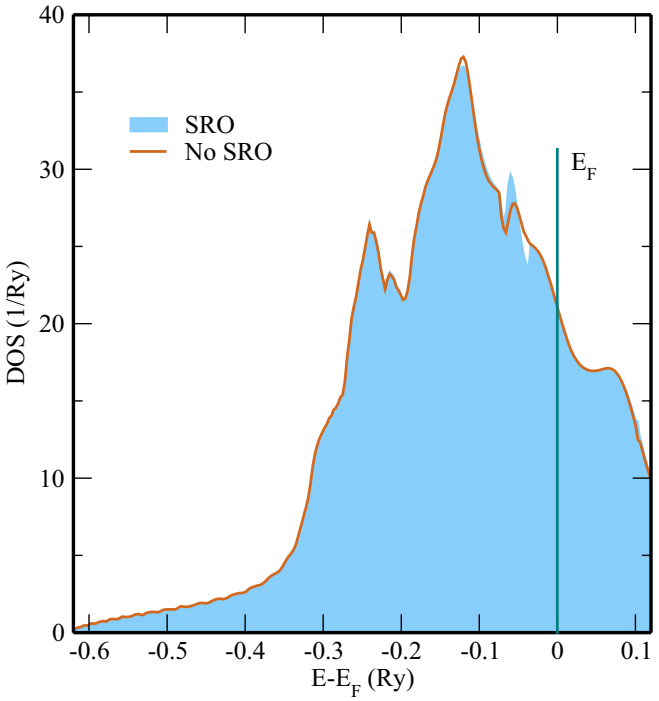

FIG. 4. (Color online) Density of states in the $Ni_{0.67}Cr_{0.33}$ random alloy obtained from the LSGF with and without atomic SRO. See text for details.

B. Effective chemical interactions in NiCr

The difference in the occupation of the d states in Ni and Cr means that the ECI in this system can strongly depend on the alloy composition. To demonstrate that it is indeed the case, we calculate the Fourier transforms of the effective chemical pair interactions, $V(\mathbf{q})$, on the fcc lattice for three different alloy compositions: $Ni_{0.2}Cr_{0.8}$, $Ni_{0.5}Cr_{0.5}$, and $Ni_{0.8}Cr_{0.2}$. The results are shown in Figs. 5–7. As one can see, not only the value of $V(\mathbf{q})$ differs in all three cases, but, more importantly,

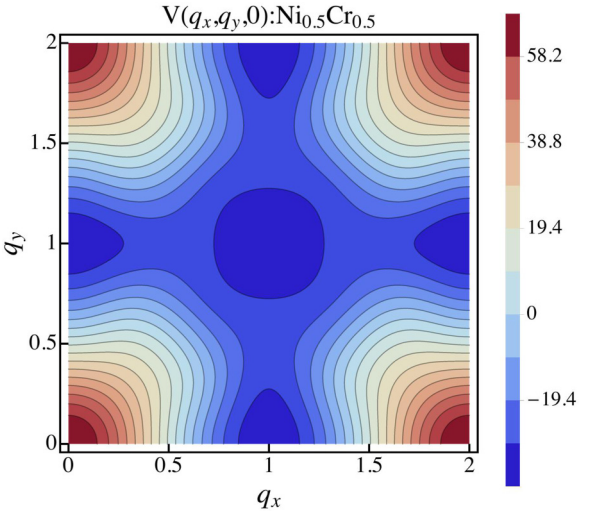

FIG. 6. (Color online) Fourier transform of the effective chemical pair interactions in $Ni_{0.5}Cr_{0.5}$ alloy in the (001) plane.

the minimum of $V(\mathbf{q})$ changes its position. This means that the type of the ordering should also be changing with the alloy composition: in the Cr-rich and equiatomic alloys, the chemical EPI should prompt the (100) type of ordering, while in the Ni-rich alloys, the ordering associated with the (0.7, 0.7, 0) point of the fcc Brillouin zone. In fact, the transition between these two types of ordering occurs somewhere close to 45 at.% of Cr.

The latter result is obviously at variance with the existing experimental data, where the $(1\frac{1}{2}0)$ type of ordering is observed in the random state. However, it is consistent with the results of Staunton *et al.* [24], who found an additional peak close to the $(\frac{2}{3}\frac{2}{3}0)$ position in the $S^{(2)}(\mathbf{q})$, which has the same meaning as $V(\mathbf{q})$, as well as in the diffuse scattering calculations for alloy compositions within concentration range of 11–33 at.% Cr. The fact that our and Ref. [24] results agree is not surprising since the methods of calculations are similar.

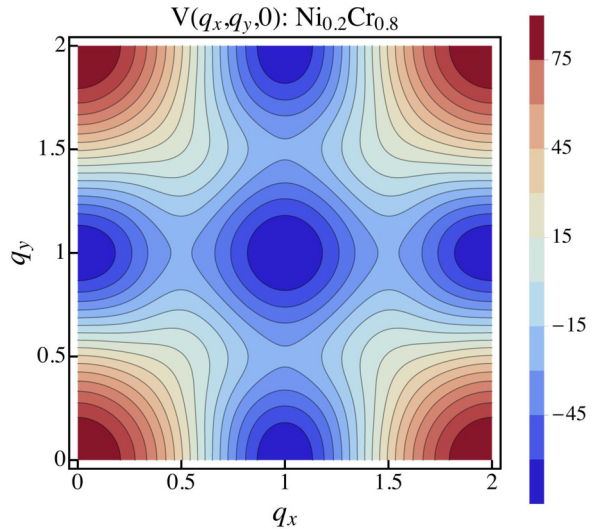

FIG. 5. (Color online) Fourier transform of the effective chemical pair interactions in $Ni_{0.2}Cr_{0.8}$ alloy in the (001) plane.

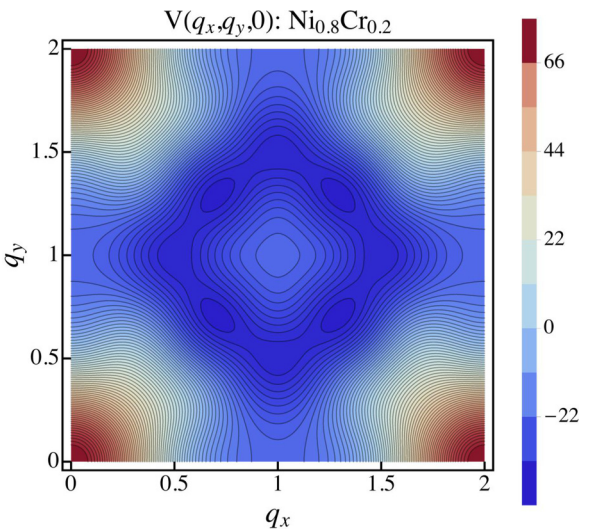

FIG. 7. (Color online) Fourier transform of the effective chemical pair interactions in $Ni_{0.8}Cr_{0.2}$ alloy in the (001) plane.

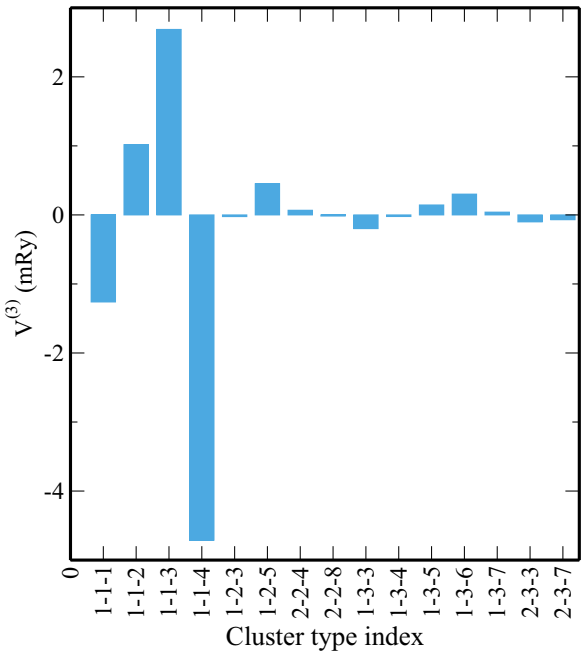

FIG. 8. (Color online) Some of the strongest three-site interactions in $Ni_{0.8}Cr_{0.2}$ alloy.

Another consequence of the large difference of the d-band filling is the existence of strong multisite interactions. In Figs. 8 and 9, we show three- and four-site interactions in $Ni_{0.8}Cr_{0.2}$ obtained in the corresponding SGPM calculations [54]. One can see that especially strong multisite interactions are for the clusters on a line along the closed-packed [110] direction, with the sides consisting of the first, (110), fourth,(220), ninth, (330), and so on coordination shells. In particular, the strongest three-site interaction is $V^{(3)}_{1-1-4}$, (−4.7 mRy) and the strongest

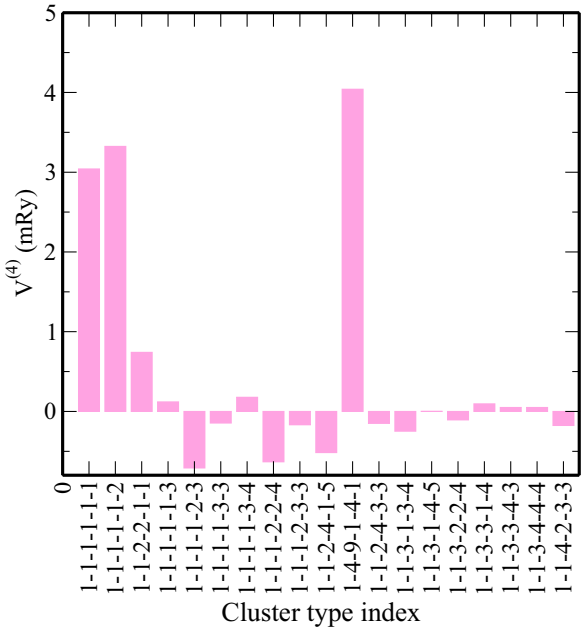

FIG. 9. (Color online) Some of the strongest four-site interactions in $Ni_{0.8}Cr_{0.2}$ alloy.

TABLE I. Ordering energies (in mRy/at) of Ni_xCr_{1-x} alloys. In the case of SGPM results, we also show the contributions from pair, three-site, and four-site interactions.

			SGPM			
x	Structure	EMTO	Total	two-site	three-site	four-site
0.50	A2B2	1.61	−0.4	−3.4	0.0	3.00
	$L1_0$	−1.58	−4.14	−4.18	0.0	0.04
0.67	Pt_2Mo	−5.45	−6.18	−3.29	−3.30	0.41
	$L1_2$	5.99	0.97	−2.01	2.51	0.47
0.75	DO_{22}	−1.89	−3.21	−2.82	−0.10	−0.21
	DO_{60}	−3.03	−3.92	−2.31	−1.44	−0.18
0.80	$D1_a$	−2.12	−3.11	−2.14	−0.65	−0.32

four-site interaction is $V^{(4)}_{1-4-9-1-4-1}$ (4.04 mRy). Let us note that this is a very general feature of the ECI in transition metal alloys, which is discussed in Ref. [55].

C. Ordering energies and trends from the ECI in Ni-Cr

To demonstrate the impact of multisite interactions upon the configurational energetics, we calculate the ordering energy of some fcc based structures with the (001) and $x(1\frac{1}{2}0)$ types of ordering. In Table I, we show the ordering energies of the A2B2 [27], $L1_0$, Pt_2Mo, $L1_2$, DO_{22}, DO_{60} [53], and $D1_a$ structures obtained using the strongest ECIs, which include the first 30 coordination shells, 75 three-site, and 26 four-site SGPM interactions and determined in the direct total energy calculations, as the energy difference of these structures and the corresponding random alloys on the ideal fcc underlying lattice.

The multisite interactions have been chosen for the clusters within of a certain range, with the exception for those, which are on the line in the closed-packed direction (like $V^{(4)}_{1-4-9-1-4-1}$). Of course, it does not guarantee that we have chosen all the most important interactions [56], nevertheless, we believe that our choice is good enough to reproduce qualitative picture of ordering in the system.

As one can see in Table I, the $L1_0$ structure, which is of the (100) type, is more stable than A2B2, which is of the $(1\frac{1}{2}0)$ type, for equiatomic alloy composition, $Ni_{0.5}Cr_{0.5}$. One can also notice that the four-site interactions yield practically the same contribution as the pair interactions, but with the opposite sign in the case of A2B2 structure, practically compensating it. Although the ordering energy obtained from the ECI is in a large error for both structures, the energy difference of these two ordered structures is reproduced reasonably well by the SGPM interactions: 3.74 mRy in the SGPM calculation and 3.14 mRy in the total energy calculations.

With increasing concentration of Ni, the type of ordering changes and in the case of an $Ni_{0.75}Cr_{0.25}$ alloy, the $L1_2$ structure, which is of the (100) type, becomes unstable. The DO_{22} structure, which is usually considered as $(1\frac{1}{2}0)$ type, but in fact it has a bit of the (100) type too, is substantially more stable than the $L1_2$. However, even more stable is the DO_{60} structure, which is of pure $(1\frac{1}{2}0)$ type [53]. One can notice that the three-site interactions yield a substantial contribution to the ordering energies of Ni_3Cr alloys in fact stabilizing the

DO_{60} against the DO_{22} and making $L1_2$ structure completely unstable.

There is a similar strong stabilizing contribution from the three-site interactions in the case of $D1_a$ structure, which is of the $\frac{4}{5}(1\frac{1}{2}0)$ type. The most interesting result is, however, for the ordering energy of the Pt_2Mo structure, which is of the $\frac{4}{3}(1\frac{1}{2}0)$, or, equivalently, $(\frac{2}{3}\frac{2}{3}0)$ type. It has the lowest ordering energy among all the presented above structures, almost twice as low as that of the DO_{60} structure. In this case, the EPI and three-site interactions produce equally large contribution to the ordering energy. The strong stabilization of this structure is consistent with the fact that the global minimum of the Fourier transform of the effective chemical pair interactions, $V(\mathbf{q})$, for this alloy composition is at (0.71, 0.71, 0) position, which is very close to $(\frac{2}{3}\frac{2}{3}0)$, similar to $V(\mathbf{q})$ in $Ni_{0.8}Cr_{0.2}$ alloy.

D. Enthalpies of formation of Ni-rich Ni-Cr alloys

In order to determine which of those phases presented in Table I structures can be stable, we have also calculated their enthalpies of formation in the *nonmagnetic* state relative to bcc Cr and fcc Ni using the PAW method, as described above. The results are presented in Fig. 10. Let us note that there exist a number of first-principles results for the formation enthalpy of Ni_2Cr in the Pt_2Mo structure, which are scattered from -6.62 to -11.59 [57] kJ/mole, and which are collected in Ref. [58]. The experimental enthalpy at 773 K is expected to be higher than that at 0 K due to incomplete long-range order.

The interesting point is that it seems that $D1_a$ structure should be stable in this system for alloy compositions close to 20 at.% Cr, at least above the Curie temperature. This is very similar to the Ni-Mo system, which is isoelectronic to Ni-Cr. However, the ordering transition temperatures are much lower in the Ni-Cr alloys and this can be the reason why $D1_a$ phase is not observed in this system.

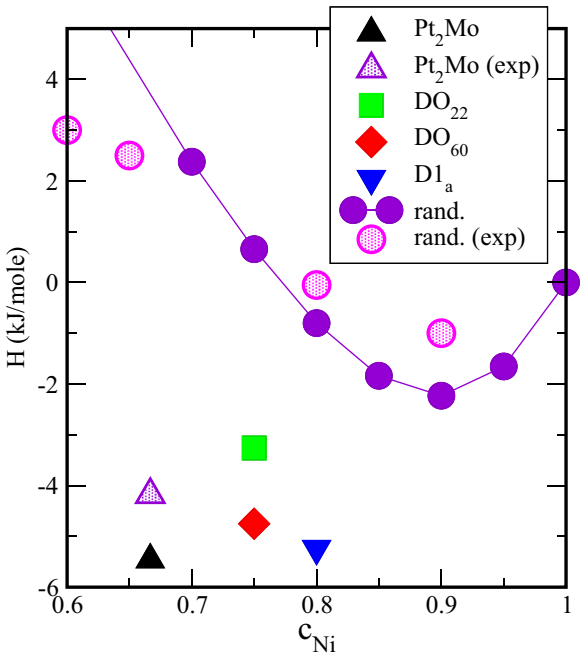

FIG. 10. (Color online) Calculated 0 K enthalpies of formation of ordered (by the PAW method) and random (by the EMTO-CPA method) of Ni-Cr alloys. The experimental data for Pt_2Mo at 773 K are taken from Ref. [59] and for random alloys at 1538 K from Ref. [60].

In Fig. 10, we also show the enthalpy of formation of random Ni-Cr alloys at 0K determined in the EMTO-CPA calculations. They do not include the contribution from local lattice relaxations. However, in separate 64-atom supercell calculations for random alloy configurations up to the 8th coordination shell by the PAW method we have found that they are -0.5 kJ/mole for $Ni_{0.75}Cr_{0.25}$ and -1.11 kJ/mole for $Ni_{0.5}Cr_{0.5}$. In other words, they produce just a little correction to the CPA results. In this figure, we also show the experimental data from Ref. [60]. However, they are for quite high temperature of about 1500 K, and thus it is expected that they can different from theoretical results.

The important message here is that the enthalpy of formation of random Ni-Cr alloys deviates quite strongly from the usual paraboliclike behavior with minimum (or maximum) at the equiatomic composition. The shift of the minimum to high Ni concentrations explains the relatively high stability of the $D1_a$ structure. At the same time, being almost as stable as Ni_2Cr, it has substantially weaker driving force for atomic ordering. This means that although the $D1_a$-Ni_4Cr phase should be stable at low temperatures, the mechanism of the phase transition, i.e., whether it is directly formed from random alloy or from some intermediate ordered phase, is unclear.

E. Configurational dependence of the ECI in Ni-Cr

As has been shown above, the SGPM interactions provide a qualitatively correct picture of ordering tendencies. However, they somehow overestimate the ordering energy by about 1–2 mRy, and they fail in the case of the ordering energy of the $L1_2$-Ni_3Cr. Therefore there is an important question: to which extent the results obtained by the SGPM can be trusted and what is the reason for the disagreement.

The first and main reason is, of course, the fact that the CPA, which is used in the SGPM calculations, has some problems as has been demonstrated above. However, the local environment effects, which are not properly described by the CPA in this system, can effect only nearest-neighbor interactions. In general, it is quite difficult to check such effects because the SGPM is built upon the CPA. However, the LSGF method allows one not only to test the effect of the local environment effects on the electronic structure, but also to obtain the ECI for atoms with a specific local environment in the random alloy.

In the isomorphous model of a random alloy, which is the case of the usual CPA, all the Ni and all the Cr atoms are identical since their local environment is exactly the same, given by the CPA effective medium. In real life, however, all the atoms of the same component are different (in terms of their local electronic structure) due to the difference of their local chemical environment. This can be modeled in supercell LSGF calculations, using a polymorphous model of a random alloy. Choosing different atoms in the supercell then one can check the effect of the local environment effects on the ECI. If the ECI depend on the choice of the atoms, there exists not only the the problem with the CPA but also with the Ising type statistical modeling in general.

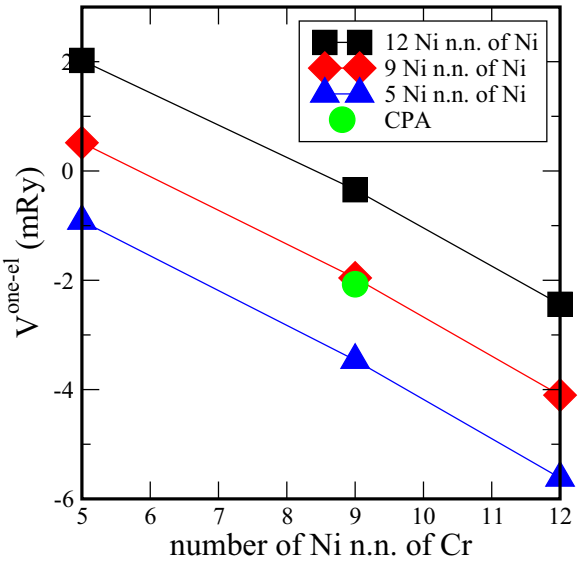

FIG. 11. (Color online) One-electron contribution to the EPI at the first coordination shell in random $Ni_{0.75}Cr_{0.25}$ alloy as a function of the number of Ni nearest neighbors. The CPA result is shown by filled circle.

In Fig. 11, we show the one-electron contribution to the chemical EPI at the first coordination shell, $V_1^{\text{one-el}}$ in a random $Ni_{0.75}Cr_{0.25}$ alloy obtained in the LSGF calculations of 256-atom supercell as a function of the number of the nearest neighbors of Cr and Ni atoms. As one can see, the interactions show strong dependence on the local environment. On the other hand, it is also clear that the ordinary CPA calculations work quite well: they produce the result very close to that for the average number of the Ni nearest neighbors in the completely random $Ni_{0.75}Cr_{0.25}$ alloy, which is nine.

Now, taking into consideration the fact that the number of the Ni nearest neighbors in the $L1_2$-Ni_3Cr is 12 for Cr and 4 for Ni, one can see that there should be a substantial reduction of the nearest-neighbor interaction in this structure, and thus a substantial increase of the ordering energy. In other words, to obtain the correct ordering energy for the completely ordered phase from the SGPM interactions one should take into consideration their renormalization due to local environment effects in the ordered state. This is beyond the aim of this investigation, since it requires a reformulation of the whole atomic configurational part.

However, if we restrict our investigation to the ordering effects in random alloys at high temperature, we can still use the usual Ising-type Hamiltonian and the SGPM. As has been demonstrated in Fig. 11, the CPA or isomorphous model still works reasonable well on average. Therefore although the ECI can fluctuate in real alloy due to the effect of the local environment on the local electronic structure of Ni and Cr atoms, the contribution of such fluctuations to the thermodynamics should be small.

F. Effect of the strain-induced interactions upon EPI

The total and SPGM EPI for $Ni_{0.8}Cr_{0.2}$ are shown in Fig. 12. Interactions are determined for the lattice constant of

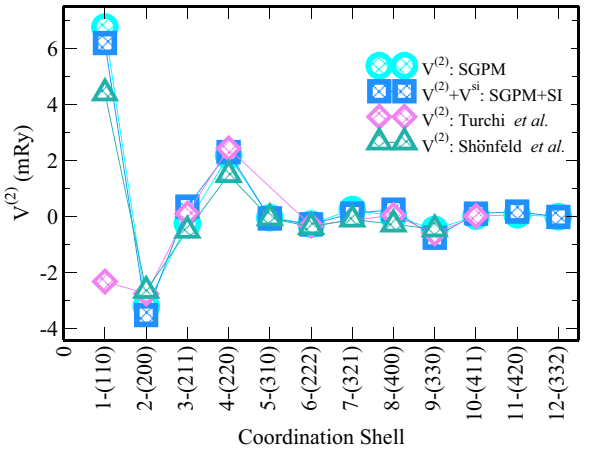

FIG. 12. (Color online) EPIs in $Ni_{0.8}Cr_{0.2}$ obtained in this work, in earlier calculations by Turchi *et al.* [23] and fitted to the experimental ASRO by Schönfeld *et al.* [20].

3.565 Å, which corresponds to the temperature of 828 K for this alloy composition [11,43,44]. The contribution from electronic excitations is included via the Fermi-Dirac distribution [61]. As one can see the contribution from the strain-induced interactions is indeed small, however, it shifts the position of the minimum of the Fourier transform of the EPI, $V_{\mathbf{q}}$ to $\mathbf{q} = (1\frac{1}{2}0)$ in accordance with the neutron diffuse scattering data.

This can be seen in Fig. 13 where we show the Fourier transform of the total EPIs for $Ni_{0.2}Cr_{0.8}$ alloy in the (001) plane. Exactly the same shift of the minimum of $V(\mathbf{q})$ due to the strain-induced interaction is also observed for $Ni_{0.67}Cr_{0.33}$ and $Ni_{0.75}Cr_{0.25}$ alloys. It is worth mentioning that we could not identify a single strain-induced interaction, which is responsible for the observed shift of the minimum of $V_{\mathbf{q}}$. One of the important contributions from the strain-induced interaction is at the seventh coordination shell. If it would change the sign of the total interaction from positive to negative, the minimum

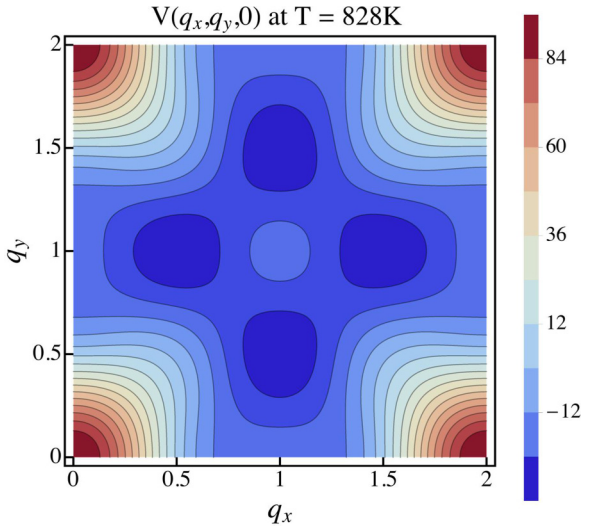

FIG. 13. (Color online) Fourier transform of the total EPI in $Ni_{0.2}Cr_{0.8}$ alloy in the (001) plane.

of $V_{\mathbf{q}}$ will be at $\mathbf{q} = (1\frac{1}{2}0)$. However, it does not, although it greatly reduces the enough strong positive chemical EPI at this coordination shell. So, the contributions from other coordination shells are also important.

Another remark concerns the fact that we use concentration independent strain-induced interactions. This is of course an approximation, but we believe that if there exists some concentration dependence of the strain-induced interactions, it should be relatively small in contrast to the one of the chemical interactions, since it is mostly related to size effect, but not to the type of the chemical bonding and complex electronic structure effects.

In Fig. 12, we also show the EPI obtained in the other GPM calculations [23] and deduced from experimental ASRO [20,21]. The agreement is quite good between all the results, except for the nearest-neighbor pair interaction in the earlier GPM calculations [23], which is quite underestimated due to the missing electrostatic contribution, as has been discussed in Ref. [24]. Note, however, that we have chosen one set of "experimental" values, although there is quite a substantial scattering of the experimental EPI for different samples [20] and also due to differences in the approximations and models used in the fitting [21].

G. Atomic SRO

The statistical thermodynamic simulations have been done by the MC method using an $18 \times 18 \times 18$ simulation box of the fcc unit cell, and a set of the ECIs consisted of the EPI at the first 25 coordination shells, 15 strongest three-site, and 13 strongest four-site interactions. We have performed 6000 MC steps per atom with 3000 steps for thermodynamic averaging to equilibrate the alloy configuration at the corresponding temperature.

In Fig. 14, we show our results for the atomic SRO in $Ni_{0.80}Cr_{0.20}$ random alloy at 828 K obtained in the MC simulations and in the diffuse scattering experiment [20]. The agreement between theory and experiment is very good, and as shown in Fig. 15, in both cases the diffuse scattering maximum is at the $(1\frac{1}{2}0)$ special point. The diffuse peaks are

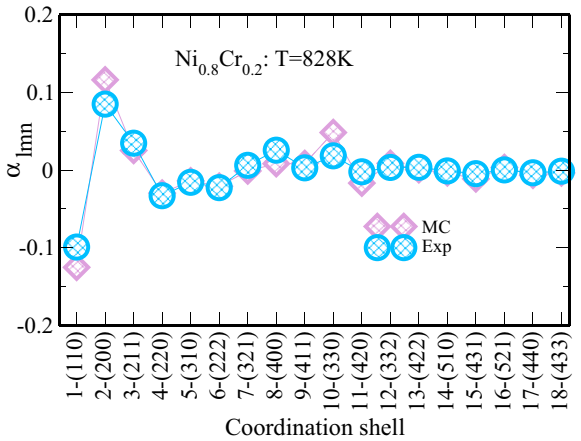

FIG. 14. (Color online) Calculated SRO parameters in $Ni_{0.8}Cr_{0.2}$ random alloy compared with experimental data from Schönfeld *et al.* [20].

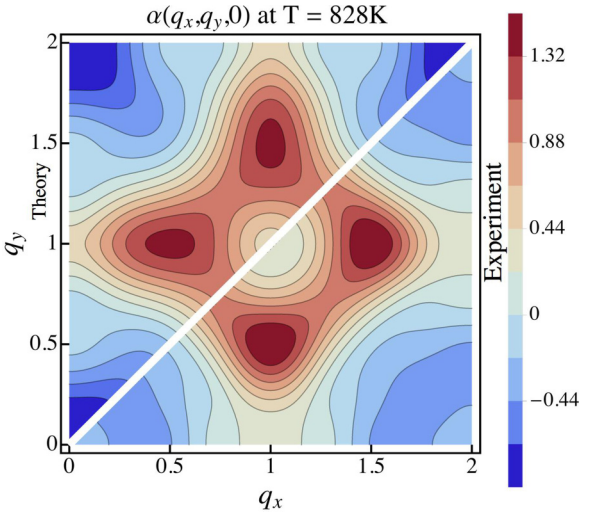

FIG. 15. (Color online) Calculated SRO diffuse intensity map, $\alpha(\mathbf{q})$, of $Ni_{0.80}Cr_{0.20}$ at 828 K in the (001) plane.

roughly triangular shaped with the edges extending towards the neighboring $D1_a$ superlattice $\frac{4}{5}(1\frac{1}{2}0)$ positions. Thus this structure could potentially be formed at lower temperatures during the first-order phase transition.

However, it is a quite nontrivial task to study such a transition using just the MC simulations, although it could take place according to our results for the formation enthalpies presented in Fig. 10. In fact, in our MC calculations, we observe actually a formation of the Pt_2Mo ordered structure. However, only a *configurational* part of the energy of an alloy is taken into consideration in our MC simulations. At the same time, as we have demonstrated above, the relatively low enthalpy of formation the $D1_a$ phase, compared to the Ni_2Cr phase is mainly due to the low enthalpy of formation of a *random* $Ni_{0.8}Cr_{0.2}$.

We have also calculated the atomic SRO and order-disorder phase transition in $Ni_{0.67}Cr_{0.33}$. The ECI for these calculations have been determined for the lattice constant of 3.596 Å, which corresponds to 1073 K [11,43,44]. In Fig. 16, we show the SRO parameters of $Ni_{0.67}Cr_{0.33}$ at 1073 K obtained in the MC calculations and determined in the neutron diffraction experiments [18]. One can see that the agreement between theoretical results and experimental data is very good, although the theoretical SRO parameters at the first two coordination shells are larger in absolute value, which also leads to a larger variations of their Fourier transform as one can see in Fig. 17 where we show $\alpha(\mathbf{q})$ in the (001) plane.

Again, as in the case of $Ni_{0.8}Cr_{0.2}$ alloy, theory correctly reproduces the position of the scattering maximum or $\alpha(\mathbf{q})$, which is $(1\frac{1}{2}0)$. After the first-order phase transition to the Pt_2Mo structure, the minimum is going to be in the $(\frac{2}{3}\frac{2}{3}0)$ point. However, such a shift most probably originates from simple geometrical rules, as the only way to have the (420) stacking for this particular alloy composition (for a thorough discussion see Refs. [12–15,62–65]).

Using these ECI, we have determined the order-disorder transition temperature in the MC simulations by cooling the system from high temperatures and monitoring the discontinuity in the average energy and peak in the heat

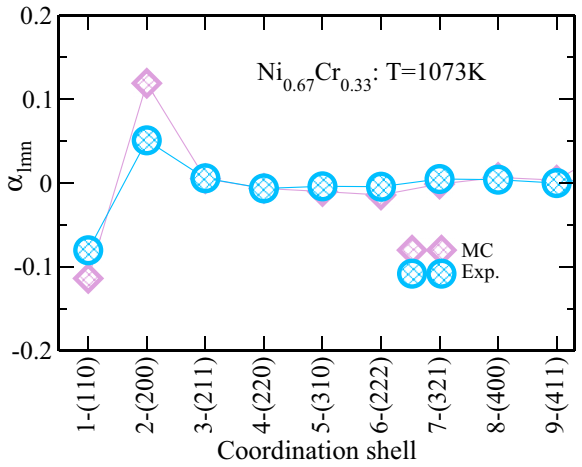

FIG. 16. (Color online) Calculated SRO parameters in $Ni_{0.67}Cr_{0.33}$ random alloy compared with experimental data from Caudron *et al*. [18].

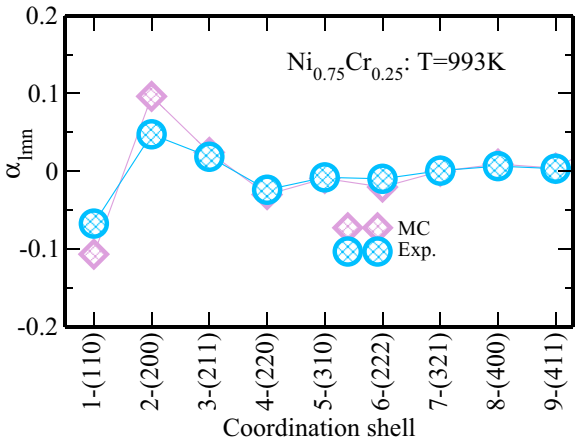

FIG. 18. (Color online) Calculated SRO parameters in $Ni_{0.75}Cr_{0.25}$ random alloy compared with experimental data from Caudron *et al*. [18].

capacity. The theoretical result 880 K is in very good agreement with the experimental value of 863 K [1,7–11]. Let us note that in spite of good agreement we believe a further investigation is needed to include possible contributions from thermal magnetic excitations and lattice vibrations. The latter, however, is quite nontrivial task especially if they should be considered together.

Finally, we calculate ASRO in $Ni_{0.75}Cr_{0.25}$ at 993 K using the ECI determined for the corresponding experimental lattice parameter of 3.578 Å [11,43,44]. The calculated SRO parameters are presented in Fig. 18 [18]. Again, as in the case of $Ni_{0.67}Cr_{0.33}$, the theoretical SRO parameters, have a larger amplitude at the first two coordination shells. At the same time, it is worth mentioning that α_{000} in the experiment are 0.935 [18], 0.843 [18], and 0.9274 [20] in $Ni_{0.67}Cr_{0.33}$, $Ni_{0.75}Cr_{0.25}$, and $Ni_{0.8}Cr_{0.2}$ alloys, respectively, which is noticeably less than 1, which is required by normalization condition (5). The later indicates that the experimental values of $\alpha(\mathbf{q})$ could be underestimated. Of course, the errors or unaccounted contributions in theoretical calculations cannot be excluded either.

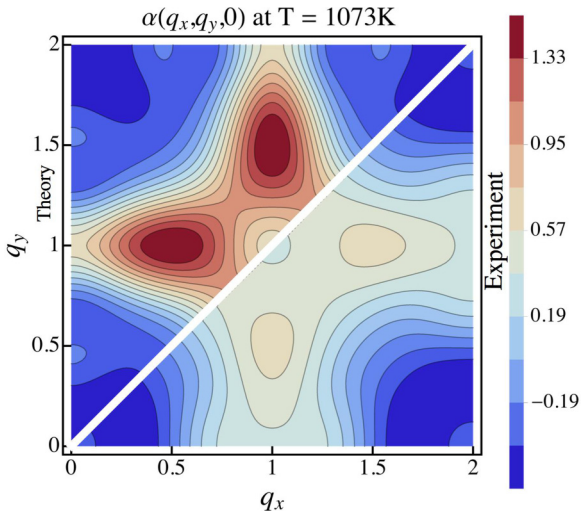

FIG. 17. (Color online) Calculated SRO diffuse intensity map, $\alpha(\mathbf{q})$, of $Ni_{0.67}Cr_{0.33}$ at 1073 K in the (001) plane.

IV. CONCLUSIONS

We have investigated the atomic ordering in the Ni-rich Ni-Cr alloys using different *ab initio* techniques and MC method. We demonstrate that the phase stability and ordering effects are quite nontrivial in this system, which is related to quite different *d*-band filling of Ni and Cr. In particular, the effective chemical interactions in this system are not only strongly concentration dependent with large multisite interactions, but they also exhibit pronounced local environment dependence, which is unusual for nonmagnetic systems.

At the same time, we have demonstrated that keeping a mean-field character of the effective interactions makes possible to obtain quantitatively accurate description of the atom ordering at high temperatures in the random state. Our effective chemical interactions turned out to be very close to those obtained long time ago by Turchi *et al*. [23] and Staunton *et al*. [24]. Although they yield the strongest and dominating contribution to the total EPI, it has turned out that the correct qualitative picture of the ASRO in the Ni-rich Ni-Cr alloys is restored only when relatively small strain-induced interactions are taken into consideration.

In spite of the fact that our results in good agreement with diffuse scattering experiment for these alloys, a further, more elaborate, first-principles investigation of this system is needed in order to address the questions related to the phase equilibrium at lower temperatures as well as to find out what is the effect of thermal magnetic and lattice vibration excitations at higher temperature. The latter is a highly nontrivial task, which cannot be efficiently addressed at the present time.

ACKNOWLEDGMENT

Authors acknowledge the financial support of the support of the Swedish Research Council (VR project 15339-91505-33) and the European Research Council (ERC) grant. This work

was partly performed within the VINNEX center Hero-m, financed by the Swedish Governmental Agency for Innovation Systems (VINNOVA), Swedish industry, and the Royal Institute of Technology (KTH). This work was supported by Russian Federation Grant 12-03-00227. Calculations have been done using UPPMAX (Uppsala), PDC (Stockholm), and NSC (Linköping) resources provided by the Swedish National Infrastructure for Computing (SNIC).

[1] P. Nash, Bull. Alloy Phase Diagrams **7**, 466 (1986).
[2] J. R. Davis, *Nickel, Cobalt and their Alloys* (ASM International, Materials Park, Ohio, 2000).
[3] K. K. Katsnelson and L. M. Shevchuk, Fiz. Met. Metalloved. **24**, 683 (1967).
[4] Y. D. Yao, Sigurds, Arajs, and E. E. Anderson, J. Low Tem. Phys. **21**, 369 (1975).
[5] N. R. Dudova, R. O. Kaibyshev, and V. A. Valitov, Fiz. Metal. Metalloved. **108**, 657 (2009).
[6] B. J. Berkowitz and C. Miller, Metall. Trans. A **11**, 1877 (1980).
[7] G. Baer, Naturwissenschaften **43**, 298 (1956).
[8] H. G. Baer, Z. Metallkd. **49**, 614 (1958).
[9] I. A. Bagariatskii and I. D. Tiapkin, Sov. Phys. Dokl. **3**, 1025 (1958).
[10] Ye. Z. Vintaykin and G. G. Urushadze, Fiz. Metall. Metalloved. **27**, 895 (1969).
[11] L. Karmazin, Mater. Sci. Eng. **54**, 247 (1982); Czech. J. Phys. B **28**, 1175 (1978); **29**, 1181 (1979).
[12] S. K. Das and G. Tomas, Phys. Status Solidi A **21**, 177 (1974).
[13] D. De Fontaine, Acta Metall. **23**, 553 (1975).
[14] G. Van Tandeloo, Mat. Sci. Eng. **26**, 209 (1976).
[15] G. Van Tandeloo, S. Amelinckx, and D. De Fontaine, Acta Cryst. B **41**, 281 (1985).
[16] Ye. Z. Vintaykin and A. A. Loshmanov, Fiz. Metall. Metalloved. **24**, 754 (1967).
[17] I. S. Belyatskaya and Ye. Z. Vintaykin, Fiz. Metall. Metalloved. **25**, 748 (1968).
[18] R. Caudron, M. Sarfati, M. Barrachin, A. Finel, F. Ducastelle, and F. Solal, J. Phys. I (France) **2**, 1145 (1992).
[19] R. Caudron, M. Sarfati, M. Barrachin, A. Finel, F. Ducastelle, and F. Solal, Physica B **180**, 822 (1992).
[20] B. Schönfeld, L. Reinhard, G. Kostorz, and W. Buhrer, Phys. Status Solidi B **148**, 457 (1988).
[21] B. Schönfeld, G. E. Ice, C. J. Sparks, H.-G. Haubold, W. Schweika, and L. B. Shaffer, Phys. Status Solidi B **183**, 79 (1994).
[22] W. Schweika and H. G. Haubold, Phys. Rev. B **37**, 9240 (1988).
[23] P. E. A. Turchi, F. J. Pinski, R. H. Howell, A. L. Wachs, M. J. Fluss, D. D. Johnson, G. M. Stocks, D. M. Nicholson, and W. Schweika, Mat. Res. Soc. Symp. Proc. **166**, 231 (1990).
[24] J. B. Staunton, D. D. Johnson, and F. J. Pinski, Phys. Rev. B **50**, 1450 (1994).
[25] A. V. Ruban and H. L. Skriver, Phys. Rev. B **66**, 024201 (2002); A. V. Ruban, S. I. Simak, P. A. Korzhavyi, and H. L. Skriver, *ibid.* **66**, 024202 (2002).
[26] A. V. Ruban, S. Shallcross, S. I. Simak, and H. L. Skriver, Phys. Rev. B **70**, 125115 (2004).
[27] F. Ducastelle, *Order and Phase Stability in Alloys* (North-Holland, 1991).
[28] P. E. Blöchl, Phys. Rev. B **50**, 17953 (1994).
[29] A. G. Khachaturyan, *The Theory of Structural Transformations in Solids* (Wiley, New York, 1983).
[30] M. A. Krivoglaz and A. A. Smirnov, *The theory of Order-Disorder in Alloys* (MacDonal and Co., 1964), p. 345.
[31] P. C. Clapp and S. C. Moss, Phys. Rev. **142**, 418 (1966).
[32] P. C. Clapp and S. C. Moss, Phys. Rev. **171**, 754 (1968).
[33] R. V. Chepulskii and V. N. Bugaev, J. Phys.: Condens. Matter. **10**, 7309 (1998).
[34] L. Vitos, H. L. Skriver, B. Johansson, and J. Kollar, Comput. Mater. Sci. **18**, 24 (2000).
[35] L. Vitos, Phys. Rev. B **64**, 014107 (2001).
[36] L. Vitos, I. A. Abrikosov, and B. Johansson, Phys. Rev. Lett. **87**, 156401 (2001).
[37] G. Kresse and J. Hafner, Phys. Rev. B **48**, 13115 (1993); G. Kresse and J. Furthmüller, Comp. Mater. Sci. **6**, 15 (1996).
[38] P. Hohenberg and W. Kohn, Phys. Rev. **136**, B864 (1964).
[39] J. P. Perdew, K. Burke, and M. Ernzerhof, Phys. Rev. Lett. **77**, 3865 (1996).
[40] Z. Arnold, J. J. M. Franse, J. Kamarad, and P. H. Frings, Physca B **128**, 201 (1985).
[41] J. P. Perdew and Y. Wang, Phys. Rev. B **45**, 13244 (1992).
[42] K. Adachi, *1.2.3.11 Ni-Cr*, edited by H. P. J. Wijn, Springer Materials: The Landolt-Börnstein Database.
[43] A. S. Pavlovic, V. S. Babu, and M. S. Seehra, J. Phys.: Condens. Matter **8**, 3139 (1996).
[44] G. A. Dosovitskiy, S. V. Samoilenkov, A. R. Kaul, and D. P. Rodionov, Int. J. Thermophys. **30**, 1931 (2009).
[45] B. L. Gyorffy, Phys. Rev. B **5**, 2382 (1972).
[46] P. Soven, Phys. Rev. **156**, 809 (1967).
[47] I. A. Abrikosov, A. M. N. Niklasson, S. I. Simak, B. Johansson, A. V. Ruban, and H. L. Skriver, Phys. Rev. Lett. **76**, 4203 (1996); I. A. Abrikosov, S. I. Simak, B. Johansson, A. V. Ruban, and H. L. Skriver, Phys. Rev. B **56**, 9319 (1997).
[48] H. J. Monkhorst and J. D. Pack, Phys. Rev. B **13**, 5188 (1976).
[49] M. A. Krivoglaz and E. A. Tikhonova, Ukr. Fiz. Zh. **3**, 297 (1958); M. A. Krivoglaz, *X-ray and Neutron Diffraction in Nonideal Crystals* (Springer-Verlag, Berlin, 1996); *Diffuse Scattering of X-rays and Neutrons by Fluctuations* (Springer-Verlag, Berlin, 1996).
[50] A. G. Khachaturyan, Sov. Phys. Crystallogr. **10**, 248 (1965); *Theory of Structural Transformations in Solids* (Wiley, New York, 1983).
[51] H. E. Cook and D. deFontaine, Acta Metall. **17**, 915 (1969).
[52] A. V. Ruban, V. I. Baykov, B. Johansson, V. V. Dmitriev, and M. S. Blanter, Phys. Rev. B **82**, 134110 (2010).
[53] O. E. Peil, A. V. Ruban, and B. Johansson, Phys. Rev. B **79**, 024428 (2009).
[54] The interaction index is given by the coordination shell numbers of the sides of the corresponding cluster. In the case of the four-site interactions, the order of indexes matters, so the choice is the following: the first four indexes are the coordination shells of the sides of a closed loop through all the four sites, and the last two are the coordination shells of remaining sides of the cluster.

[55] A. Bieber and F. Gautier, J. Phys. Soc. Jpn. **53**, 2061 (1984).
[56] An example of strong three-site interactions for a relatively large clusters are, for instance, $V^{(3)}_{4-4-17}$ and $V^{(3)}_{1-9-17}$, which are 0.43 and 0.46 mRy, respectively, in $Ni_{0.8}Cr_{0.2}$ alloy. Here, the 17th coordination shell is (440). Let us note that the pair effective interaction at the 17th coordination shell is −0.15 mRy.
[57] A. Arya, G. K. Dey, V. K. Vasedevan, and S. Banerjee, Acta Mater. **52**, 3301 (2002).
[58] K. S. Chan, Y.-D. Lee, and Y.-M. Pan, Metal. Mat. Trans. A **37**, 523 (2006).
[59] M. Hirabayashi, M. Koiwa, K. Tanaka, T. Tadaki, T. Saburi, S. Nenno, and H. Nishiyama, Trans. JIM **10**, 365 (1969).
[60] A. Watson and F. H. Hayes, J. Alloys Compd. **220**, 94 (1995).
[61] N. D. Mermin, Phys. Rev. **137**, A1441 (1965).
[62] Satoshi Hata, Syo Matsumura, Noriyuki Kuwano, and Kensuke Oki, Acta Mater. **46**, 881 (1998).
[63] S. Banarjee, K. Urban, and M. Wilkens, Acta Metall. **32**, 299 (1984).
[64] U. D. Kulkarni, Acta Mater. **52**, 2721 (2004).
[65] P. R. Okamoto and G. Thomas, Acta Metall. **19**, 825 (1971).